Available online at www.sciencedirect.com
ScienceDirect
Trans. Nonferrous Met. Soc. China 22(2012) 700−710
Transactions of Nonferrous Metals Society of China
www.tnmsc.cn

# Effect of micro arc oxidation treatment on localized corrosion behaviour of AA7075 aluminum alloy in 3.5% NaCl solution

A. VENUGOPAL[1], Rajiv PANDA[1], Sushant MANWATKAR[1], K. SREEKUMAR[1], L. RAMA KRISHNA[2], G. SUNDARARAJAN[2]

1. Material Characterization Division, Materials and Metallurgy Group, Vikram Sarabhai Space Centre, Thiruvananthapuram-695022, India;
2. International Advanced Research Centre for Powder Metallurgy and New Materials, Hyderabad- 500005, India

Received 20 June 2011; accepted 26 July 2011

**Abstract:** Alumina coating was formed on AA7075 aluminum alloy by micro arc oxidation (MAO) method and its corrosion and stress corrosion cracking (SCC) behaviors were examined in 3.5% (mass fraction) NaCl solution. Electrochemical impedance spectroscopy (EIS) was used to evaluate the degradation of the coating as a function of immersion time and was modeled with appropriate equivalent circuits. Constant load stress corrosion cracking (SCC) results followed by post-test metallographic observations demonstrated the usefulness of MAO coating to avoid the premature failure of the alloy due to severe localized corrosion initiated by Cu- and Fe-rich intermetallic phases.
**Key words:** aluminum alloy; micro arc oxidation; impedance spectroscopy; stress corrosion

## 1 Introduction

Localized corrosion of aluminium alloys containing intermetallic phases with elements such as Cu and Fe, has been the subject of study by several researchers [1−6]. These particles were identified as potential nucleation sites for the initiation of fatigue cracks leading to premature failure of the structures [7,8]. Hence, it is important to understand the electrochemical behaviour of aluminium having such phases and to improve the corrosion resistance using appropriate surface treatment methods. Recently, micro arc oxidation (MAO) is widely employed for coating light alloys, such as aluminum and magnesium, as a surface modification technique due to its excellent adhesion, improved wear, and corrosion resistance compared with conventional anodic film [9−11]. MAO coating usually consists of a porous outer layer and a compact inner layer in which the composition and thickness depend on the nature of electrolyte and treatment. Several studies have been carried out using this approach and the fabricated coating has been characterized in terms of microstructure, phase content and corrosion resistance [12−15]. With respect to aluminium alloys, LI et al [16] obtained hard corrosion resistant alumina coating on Al−Si alloy in borate electrolyte. Similar improvement was also achieved for other aluminium alloys, such as Al−Cu, Al−Mg and Al−Zn−Mg [10−13]. Although this treatment was shown to exhibit good corrosion and wear resistance, the electrochemical behaviour of such coatings under long-term immersion conditions was not studied in detail. Also, the stress corrosion cracking (SCC) performance of such coatings, especially for aluminium alloys, has not been examined except a few studies on magnesium alloys, such as AM50 and AZ61 [17−19]. In the present investigation, attempt has been made to study the above aspects using electrochemical impedance spectroscopy (EIS) along with constant load (CL) stress corrosion cracking tests using AA7075−T7352 alloy in 3.5% NaCl solution.

## 2 Experimental

### 2.1 Materials

The substrate material used in the present investigation was AA7075−T7352 aluminium alloy forging having the chemical composition of (mass fraction): 1.2% Cu, 5.1% Zn, 2.1% Mg, 0.15% Si, <0.1% Mn, <0.2% Fe, 0.2% Cr, <0.1% Ti. The alloy was

**Corresponding author:** A. VENUGOPAL; Tel: +11-91-471-2562614; Fax: +11-91-471-2705048; Email: arjun_venu@hotmail.com
DOI: 10.1016/S1003-6326(11)61234-X

solution treated at 470 °C for 36 h and water quenched to room temperature. Subsequently two-step aging was performed at 107 °C for 8 h and 177 °C for 8 h, respectively. Flat rectangular specimens having effective gauge dimensions of 30 mm×6 mm×4 mm were used for tensile tests, which were tested at a crosshead speed of 2 mm/s. The mechanical properties of this alloy in the above heat-treated condition were 0.2% yield strength of 320 MPa, ultimate tensile strength of 425 MPa and elongation of 11.2%. MAO coating was generated on the actual tensile specimens on all four sides of the gauge length portion.

### 2.2 MAO coating process

An alkali silicate solution (4 g/L KOH, 2 g/L $Na_2SiO_3$) was used as an electrolyte and the coating process was carried out at a constant current density of 0.2 A/cm$^2$ using a specially designed 50 Hz frequency AC high voltage power supply. The temperature of the electrolyte was maintained constant at 35 °C using a heat exchanger throughout the coating process. The treatment time of the samples was 30 min. The samples were taken out of the electrolyte, thoroughly washed in cold running water, ultrasonically cleaned in the acetone medium and dried.

### 2.3 Microstructure and phase analysis

Samples were sectioned and polished down to 5 μm alumina finish followed by etching in Keller's reagent (5 mL $HNO_3$, 3 mL HCl, 2 mL HF and 190 mL distilled water) and were examined under optical and scanning electron microscopes (SEM) for microstructural observations before and after coating using Carl-Zeiss EVO−50 scanning electron microscope (SEM). X-ray diffraction analysis was performed using PANalytical model X-ray diffractometer with Cu $K_\alpha$ radiation between 30° and 120° to identify the phases present in the coating. Similar measurements were made on AA7075 alloy without coating for comparison purposes.

### 2.4 Electrochemical corrosion tests

Corrosion resistance of the uncoated and MAO coated specimens was evaluated through electrochemical impedance spectroscopy technique using computer controlled Zhaner IM6ex electrochemical workstation. Unstirred 3.5% NaCl solution prepared with distilled water that has been exposed freely to the atmosphere was used as corrosive medium. Tests were carried out using a standard three-electrode setup with Pt as counter electrode, saturated calomel electrode (SCE) as a reference. Impedance measurements were carried out on the uncoated and MAO coated specimens in the frequency range of $10^5$−$10^{-2}$ Hz with an amplitude ±10 mV. The time dependant behaviour of the coating was examined by acquiring the spectra over different time intervals (0.5, 48, 96, 144 and 192 h).

### 2.5 Stress corrosion cracking (SCC)

Stress corrosion tests were carried out using constant load method by subjecting the uncoated and coated tensile specimens to 80% of the yield strength (YS) for a period of 30 d. The specimens were continuously immersed in the electrolyte throughout the test period using constant load proof rings supplied by CORTEST. Tests were also carried out on the uncoated specimens by pre-exposing them in the corrosive environment without any load for the same period as that of the SCC test (30 d). Tensile test was followed to separate the electrochemical corrosion effect such as pitting on SCC. Acrylic containers were used to hold the specimen in the environment. Flat rectangular specimens having effective gauge dimensions of 30 mm×6 mm×4 mm were used for SCC tests, in which the MAO coating was provided within the gauge length. Before coating, the gauge length portion of the samples was polished up to 1000 grit SiC paper on all the sides to obtain a smooth surface. Then, they were degreased in acetone and cleaning in distilled water. Observations were made periodically for any failure of the specimens. In the case of no failure, the specimens were further subjected to mechanical test to measure the reduction in mechanical parameters (if any) as a result of immersion in 3.5% NaCl solution. Two specimens were used for both coated and un-coated specimens and the average of the two values was taken.

## 3 Results

### 3.1 Microstructure and morphology of coating

The microstructure of AA7075 aluminum alloy observed under optical (OM) and scanning electron microscope (SEM) is shown in Fig. 1. Second phase particles appearing as black in colour are evident (Fig. 1(a)). The sizes of the particles are in the range of 2−5 μm and are present preferentially along the grain boundaries (Fig. 1(b)). These phases were well studied and reported as $Al_7Cu_2Fe$, and $(Al,Cu)_6(Fe,Cu)$ intermetallic phases in commercial 7000 series aluminum alloys in addition to fine strengthening precipitates of $MgZn_2$ [1−6]. The surface morphology of the ceramic alumina coating generated on this alloy along with the coating cross section is presented in Fig. 2. Micro pores of diameter less than 5 μm are evident on the coating and are characteristic of such plasma electrolytic oxidation (PEO) ceramic coatings (Fig. 2(a))

[20,21]. The coating thickness is of the order of 30 μm as seen from the cross-sectional SEM image (Fig. 2(b)). It can be noted that the coating exhibits a bi-layer structure with an outer porous (15 μm) layer and an inner compact (15 μm) layer.

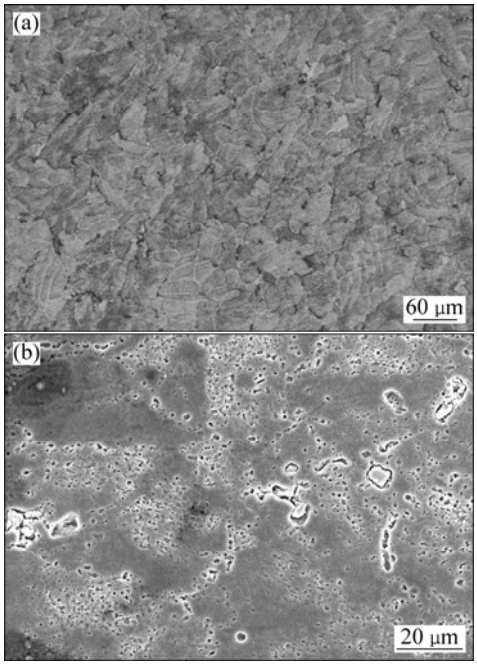


**Fig. 1** Optical (a) and SEM (b) micrographs of AA7075−T7352 alloy

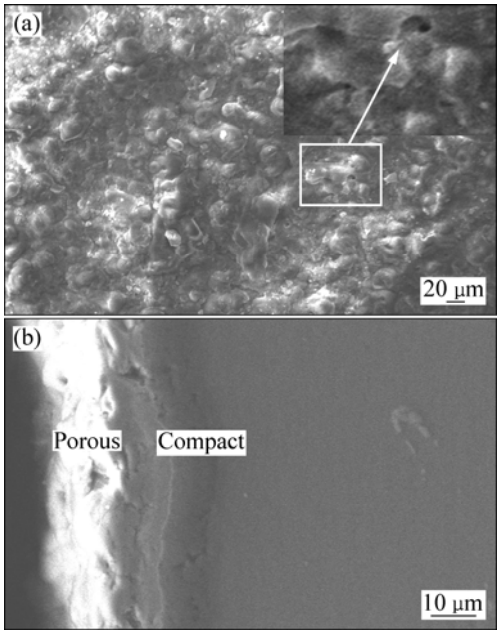


**Fig. 2** SEM micrographs showing surface morphology (a) and cross-section (b) PEO coating

### 3.2 Phase analysis

X-ray diffraction (XRD) pattern obtained from the ceramic alumina coating is exhibited in Fig. 3 along with the pattern obtained for the base metal. Analysis of the XRD patterns revealed that the component of the coating layer is mainly $\gamma$-$Al_2O_3$. The presence of aluminium peak could be due to the penetration of X-ray into the substrate.

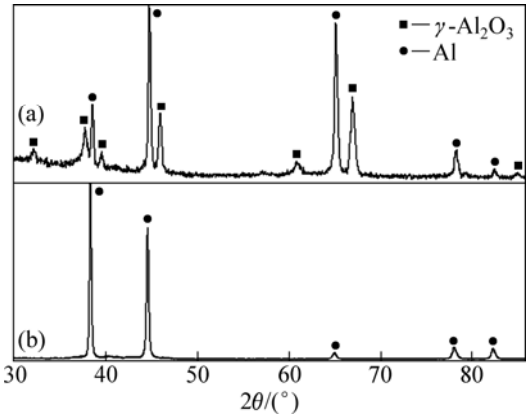


**Fig. 3** XRD patterns of PEO coating formed on AA7075 alloy (a) and base alloy (b)

### 3.3 Electrochemical impedance spectroscopy (EIS)

The corrosion behaviour of the uncoated and coated specimens was examined using EIS as a function of exposure time in 3.5% NaCl solution. The impedance data obtained for the uncoated base metal over different periods are displayed in Fig. 4 in the form of both Nyquist and Bode plots. The experimental data were fitted using appropriate equivalent circuits within the limits of experimental error (<3%), and the fit results corresponding to immersion times of 0.5 h and 192 h are shown in Figs. 4 (f) and (g). These plots exhibit two time constants up to 96 h immersion time and later turn into a single semicircle with an inductive loop in the low frequency region (144 and 192 h). The high frequency semicircle represents the dielectric behaviour of the passive film on the base metal while the low frequency spectra correspond to the metal dissolution process through the defects or pores in the film [22]. The emergence of inductive loop in the low frequency region suggests the localized corrosion processes incorporating the chloride ions [15]. The equivalent circuits used to fit the experimental plots are shown in Fig. 5. In the equivalent circuits, $R_s$ is the solution resistance, $R_f$ is the film resistance with constant phase element CPE1 and $R_{ct}$ is the charge transfer resistance with constant phase element CPE2. Instead of a capacitance, constant phase element (CPE) was used due to the porous and inhomogeneous nature of the coating. $R_L$ is the charge transfer resistance due to localized corrosion with the inductance $L$. The obtained impedance parameters are summarized in Tables 1 and 2.

It can be observed from Table 1 that, both the $R_f$ and $R_{ct}$ values are quite high during the initial exposure time and significantly reduce after 0.5 h of immersion.

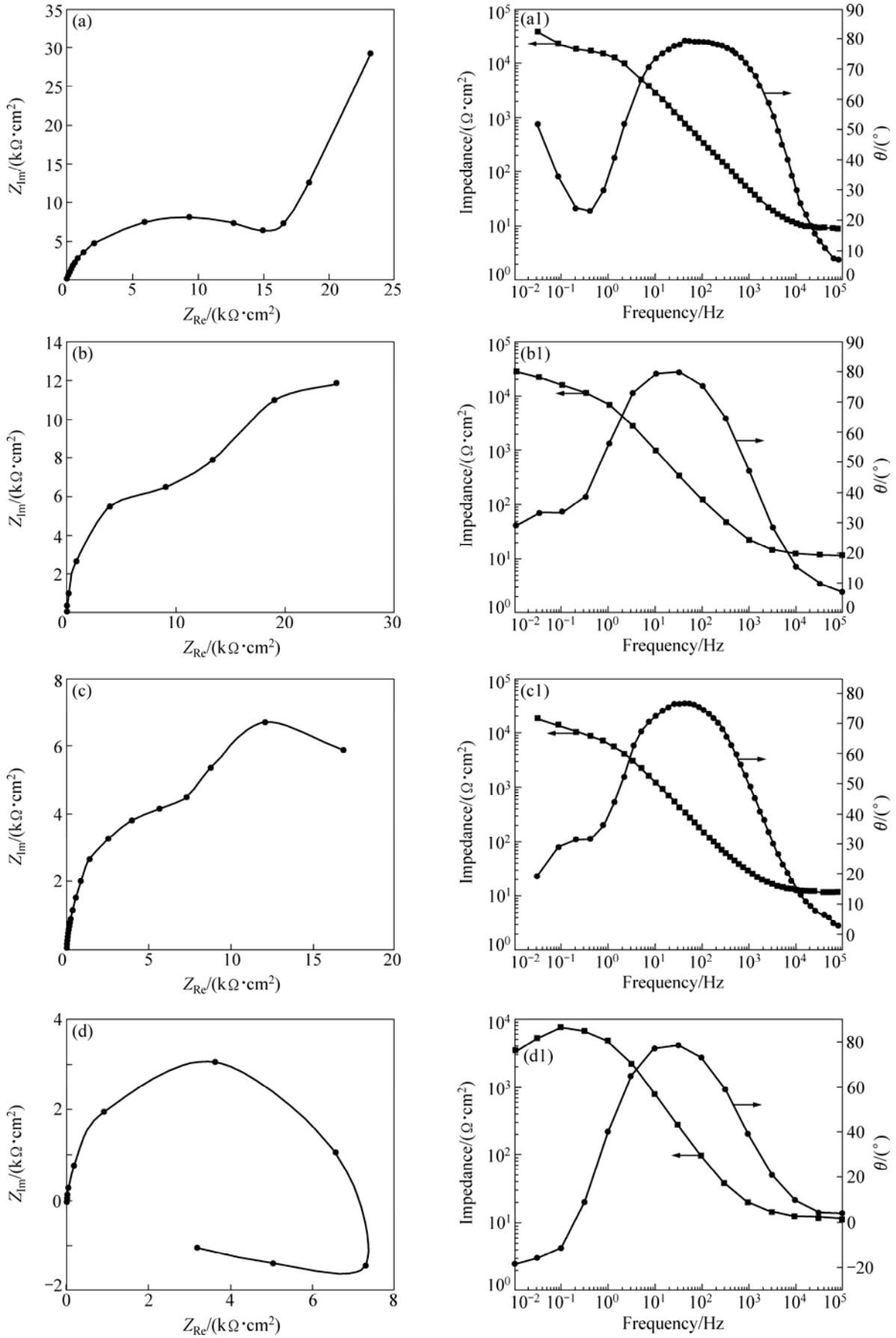
(a)
(a1)
(b)
(b1)
(c)
(c1)
(d)
(d1)
$Z_{Im}/(k\Omega\cdot cm^2)$
$Z_{Re}/(k\Omega\cdot cm^2)$
Impedance/$(\Omega\cdot cm^2)$
$\theta/(^\circ)$
Frequency/Hz

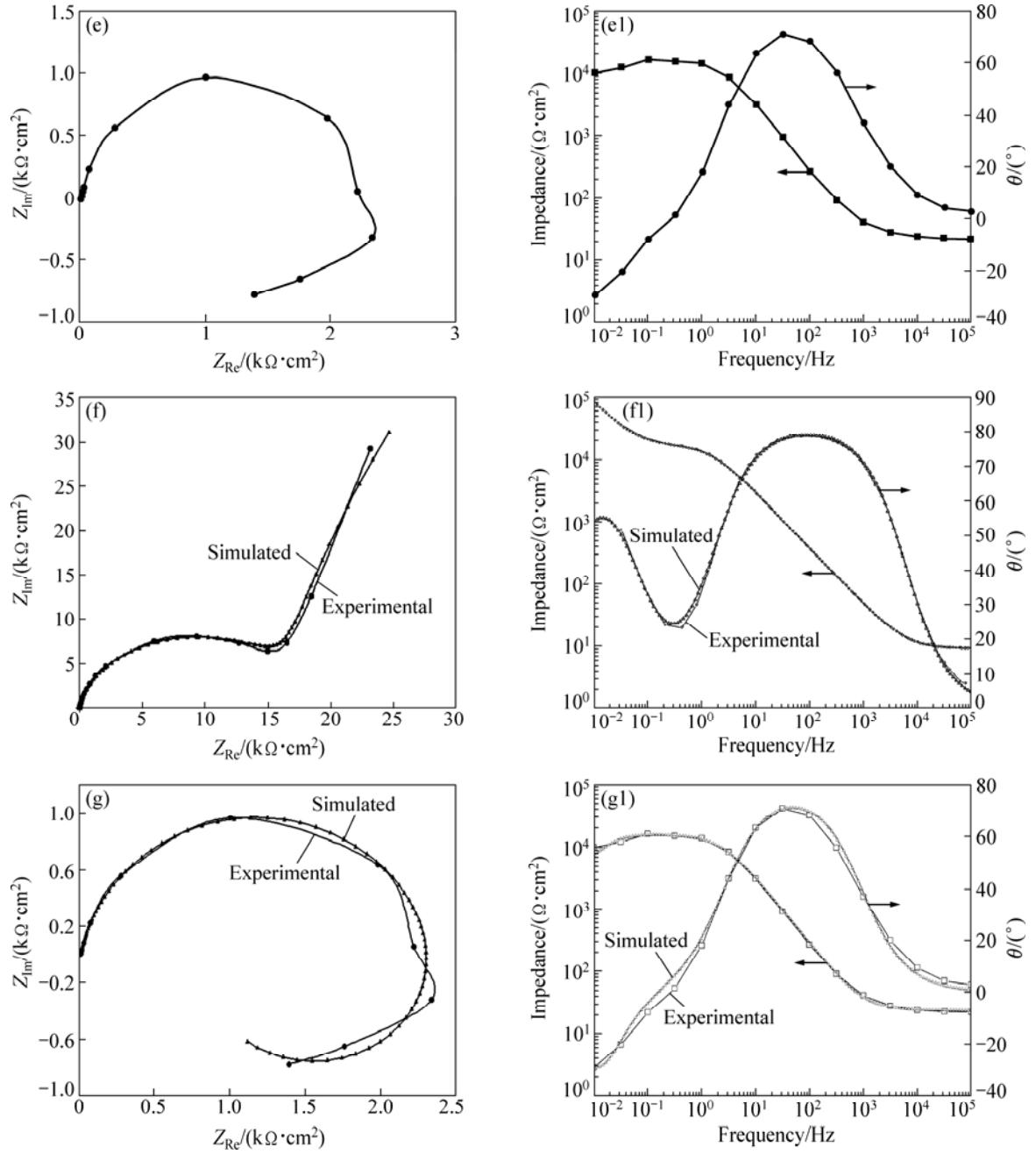


**Fig. 4** Nyquist and Bode plots showing impedance variation observed for AA7075 aluminium alloy in 3.5% NaCl solution as a function of time of 0.5 h (a, a1), 48 h (b, b1), 96 h (c, c1), 144 h (d, d1) and 192 h (e, e1), and fit result of Nyquist and Bode plots for immersion times of 0.5 h (f, f1) and 192 h (g, g1)

Corresponding increase in the CPE values can also be noted. This clearly signifies the diffusion of electrolyte through the pores and initiation of the localized corrosion within the short immersion period (0.5 h). The observation of the samples after impedance tests revealed the existence of thick corrosion product film (Fig. 6(a)) and localized corrosion initiated from the Cu- and Fe-rich particles as analyzed by EDS (Fig. 6(b)).

Contrarily, in the case of MAO coated specimen, the two time constants are evident till the end of the exposure period without any inductive features (Fig. 7). The fit results show the experimental and the simulated values corresponding to the data measured for 0.5 h and 192 h immersion period. The equivalent circuit model used to evaluate the impedance parameters is represented in Fig. 8. $R_P$ is the film resistance corresponding to the outer porous layer and the inner compact layer resistance is denoted as $R_B$. The absence of inductive features in the case of coated sample suggests that localized corrosion as noted in the case of uncoated sample did not happen.

The SEM micrograph of the coated sample observed after impedance tests confirms that the coating is intact without any localized pitting (Fig. 9). The impedance parameters obtained for the coated alloy are given in Table 3.

The variations in $R_P$ and $R_B$ values as dictated in Table 3 clearly show the poor corrosion behaviour of the outer layer as the resistance value is much lower compared with the inner compact layer ($R_B$). Although the latter also exhibits similar reduction in values with immersion time, they are found to be high compared with $R_p$ at all immersion time. The higher values of $R_B$ compared with $R_P$ at all immersion time show that the corrosion protection for the base metal is provided by only the inner compact layer not the outer porous layer. Furthermore, the lower $n$ values for both outer and inner

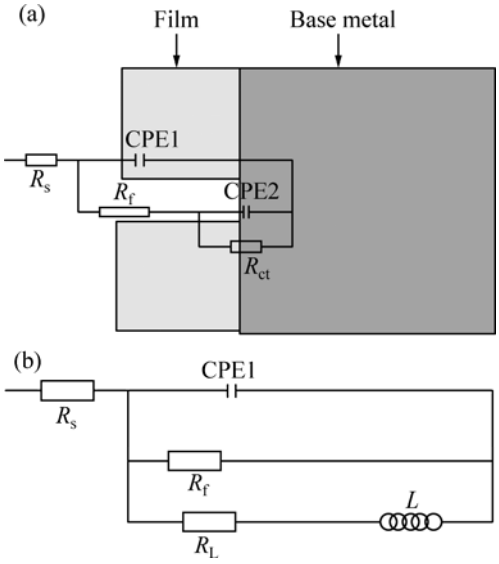


**Fig. 5** Schematic representation of AA7075 alloy together with equivalent circuit used to model impedance data corresponding to immersion time up to 96 h in 3.5% NaCl solution: (a) Up to 96 h; (b) Beyond 96 h

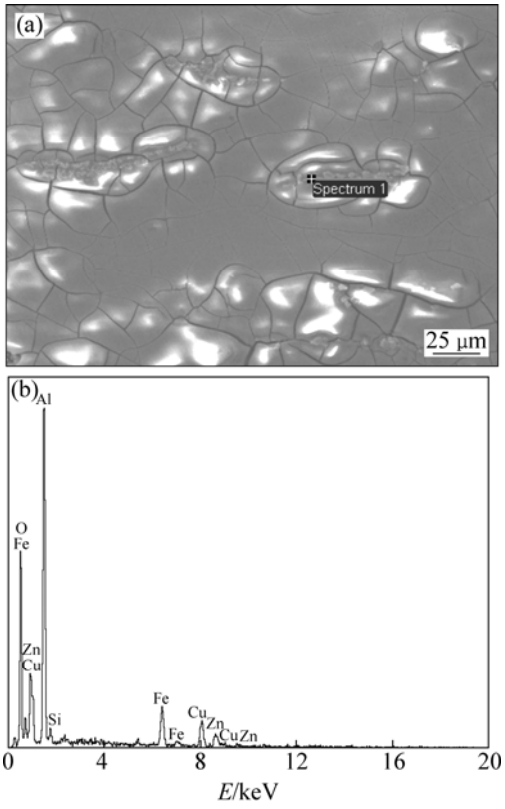


**Fig. 6** Corrosion morphology of AA7075 aluminium showing severely localized corrosion observed after impedance tests (a) and EDS spectrum (b) showing presence of Fe- and Cu-rich phases

**Table 1** Fitting results of impedance data measured for base metal up to 96 h of immersion in 3.5% NaCl solution

| Time/h | $R_f$/(kΩ·cm$^2$) | CPE1 | $n_1$ | $R_{ct}$/(kΩ·cm$^2$) | CPE2 | $n_2$ | $R_s$/(Ω·cm$^2$) |
|---|---|---|---|---|---|---|---|
| 0.5 | 19.0 | $3.4\times10^{-6}$ | 0.9 | 244 | $6.5\times10^{-5}$ | 0.9 | 9.0 |
| 48 | 14.0 | $9.8\times10^{-6}$ | 0.9 | 46 | $2.9\times10^{-5}$ | 0.9 | 12.0 |
| 96 | 9.9 | $7.4\times10^{-6}$ | 0.9 | 10 | $6.6\times10^{-4}$ | 1.0 | 12.0 |

**Table 2** Fitting results of impedance data measured for base metal beyond 96 h of immersion in 3.5% NaCl solution

| Time/h | $R_f$/(kΩ·cm$^2$) | CPE1 | $n_1$ | $R_L$/(kΩ·cm$^2$) | $L$/H | $R_s$/(Ω·cm$^2$) |
|---|---|---|---|---|---|---|
| 144 | 3.1 | $1.3\times10^{-5}$ | 0.9 | 4.0 | $1.4\times10^{4}$ | 12.0 |
| 192 | 3.0 | $1.4\times10^{-5}$ | 0.9 | 4.0 | $1.2\times10^{4}$ | 10.0 |

**Table 3** Fitting results of impedance data measured for MAO coated AA7075 alloy in 3.5% NaCl solution

| Time/h | $R_P$/(kΩ·cm$^2$) | CPE1 | $n_1$ | $R_B$/(kΩ·cm$^2$) | CPE2 | $n_2$ | $R_s$/(Ω·cm$^2$) |
|---|---|---|---|---|---|---|---|
| 0.5 | 7.5 | $0.5\times10^{-6}$ | 0.7 | 493 | $0.8\times10^{-6}$ | 0.6 | 9.0 |
| 48 | 0.4 | $2.3\times10^{-6}$ | 0.6 | 29 | $1.2\times10^{-5}$ | 0.9 | 10.4 |
| 96 | 0.03 | $4.4\times10^{-6}$ | 0.6 | 53 | $4.0\times10^{-6}$ | 0.7 | 10.0 |
| 144 | 0.1 | $5.0\times10^{-6}$ | 0.7 | 17 | $1.0\times10^{-5}$ | 0.7 | 12.0 |
| 192 | 0.1 | $4.5\times10^{-6}$ | 0.7 | 13 | $1.2\times10^{-5}$ | 0.7 | 10.2 |

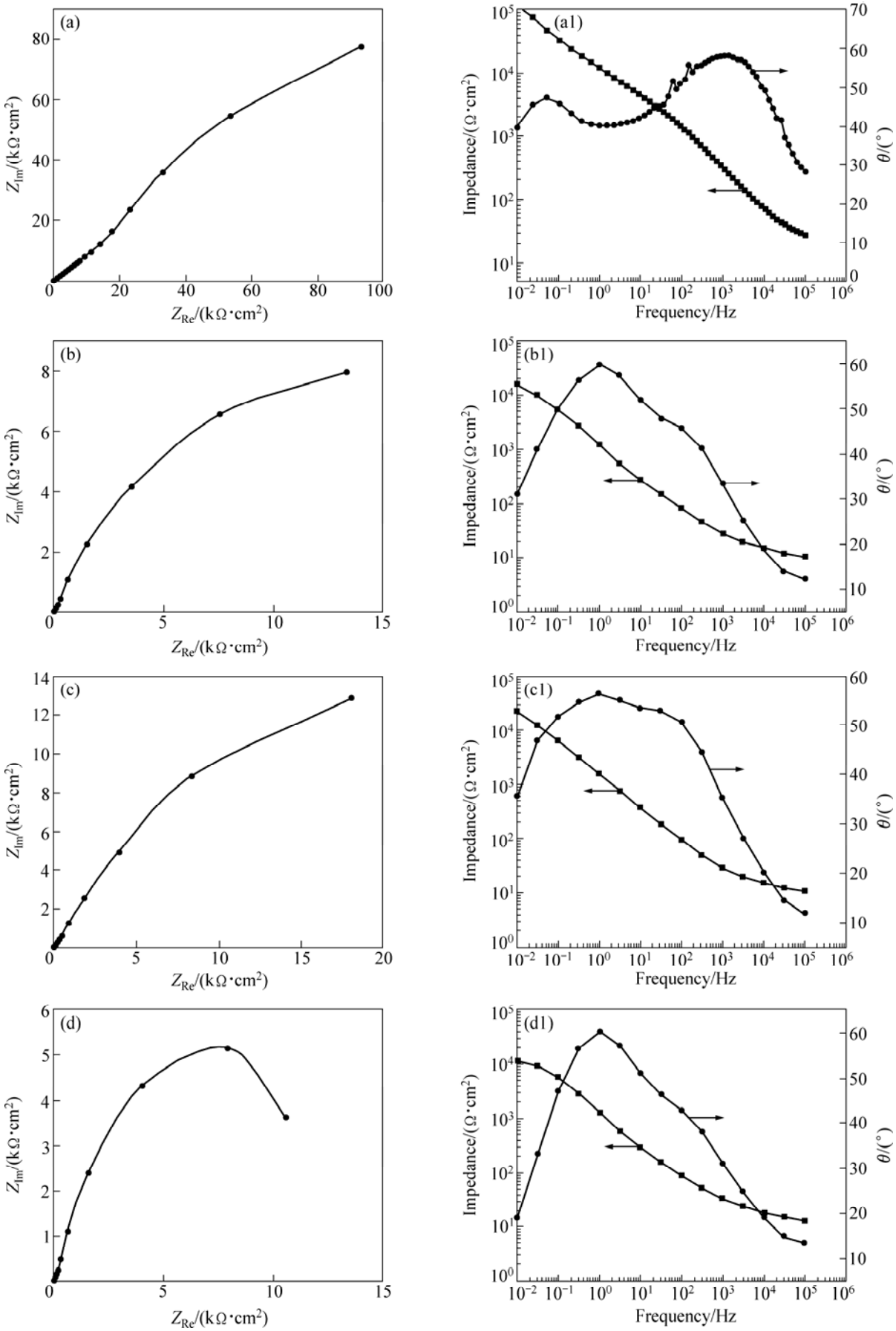
(a)
$Z_{Im}$/(kΩ·cm²)
$Z_{Re}$/(kΩ·cm²)
(a1)
Impedance/(Ω·cm²)
θ/(°)
Frequency/Hz
(b)
(b1)
(c)
(c1)
(d)
(d1)

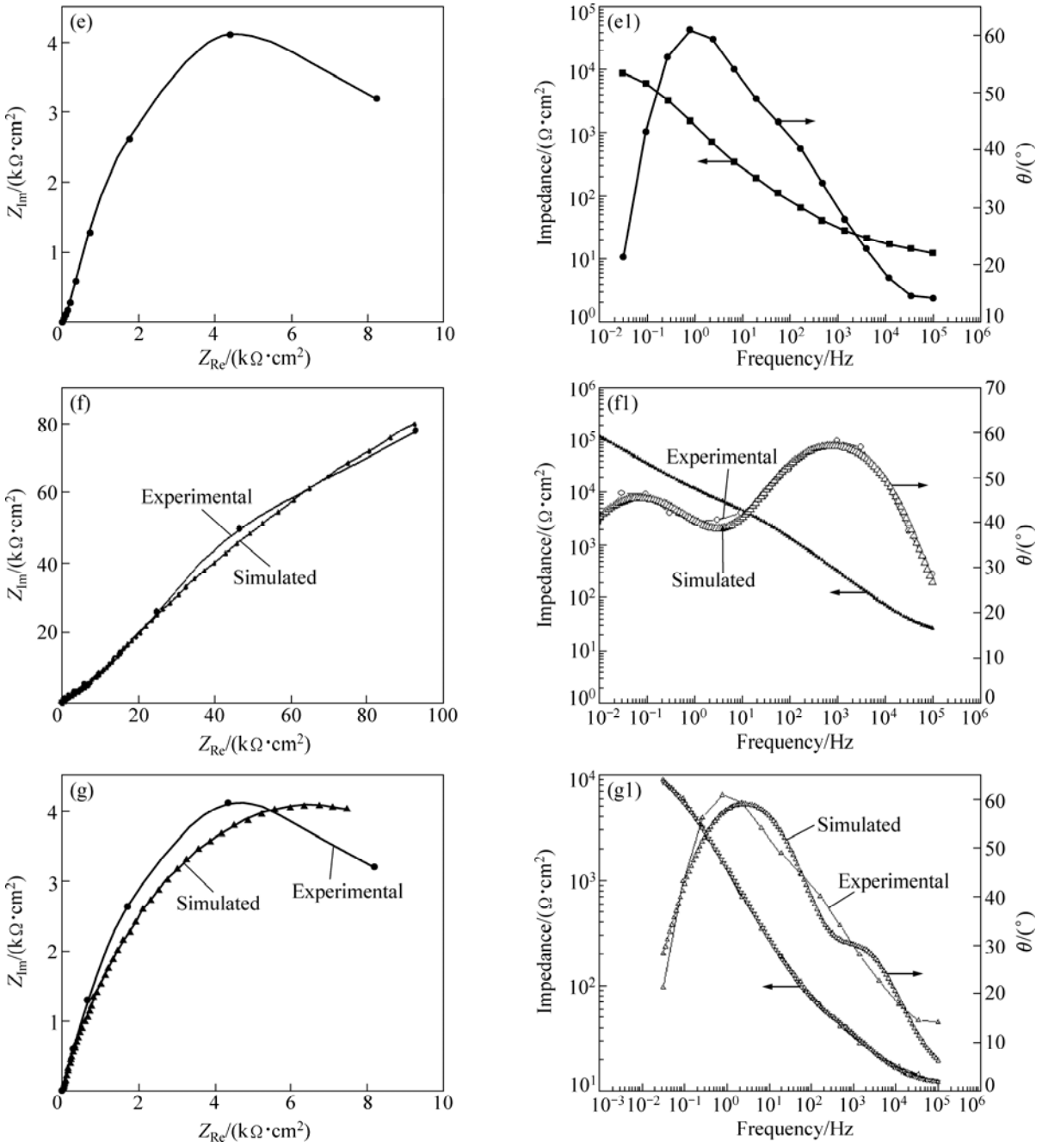


**Fig. 7** Nyquist and Bode plots showing impedance variation observed for MAO coated AA7075 aluminium alloy as function of time of 0.5 h (a, a1), 48 h (b, b1), 96 h (c, c1), 144 h (d, d1), 192 h (e, e1), and fit result of Nyquist and Bode plots for immersion time of 0.5 h (f, f1) and 192 h (g, g1)

oxide layers could be attributed to the non-uniform and porous nature of the film.

### 3.4 Stress corrosion cracking (SCC)

Table 4 summarizes the mechanical properties of the alloy tested in the as-received, un-coated and coated specimens after constant load (80% YS) SCC tests. The values shown in the table are the average of two specimens. An observation of the table indicates a drastic reduction in elongation of the specimen (11.2% to 3.5%) after exposure to constant load tests, suggesting that the alloy is susceptible to SCC. UTS values do not show any variation. But the YS values are considerably high after SCC tests. The reason for the increased values is not yet known, possibly due to hydrogen absorption in the alloy as the second phase particles are cathodic compared with matrix aluminium. However, MAO coated specimen does not show much reduction in the elongation values as exhibited by high value (10.5%). Interestingly, the specimen exposed without load and thereafter tensile tested also reveals drastic reduction in elongation (2.5%). Further examination of the tested specimens under stereomicroscope shows severely localized corrosion on the un-coated specimen and its absence in the case of

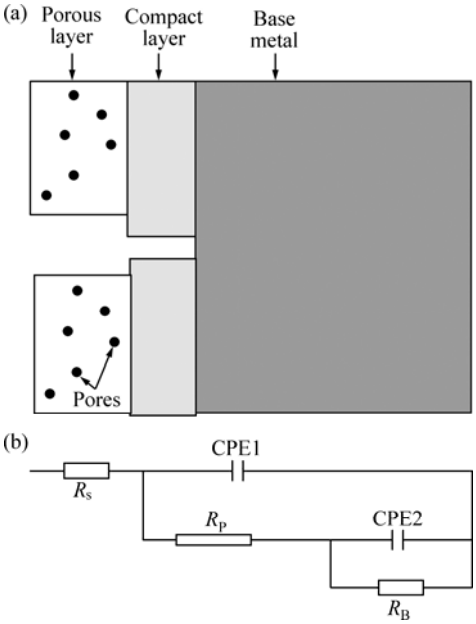


**Fig. 8** Schematic representation of MAO coated AA7075 alloy (a) together with equivalent circuit (b) used to model the impedance data at all immersion times in 3.5% NaCl solution

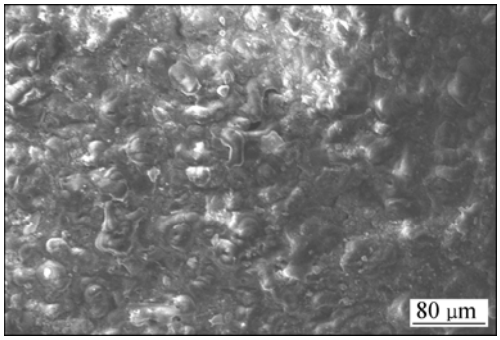


**Fig. 9** Corrosion morphology of MAO coated AA7075 aluminium alloy observed after impedance test

**Table 4** Mechanical properties of AA7075−T7352 after SCC tests

| Specimen | UTS/MPa | 0.2% YS/ MPa | Elongation (25 mm GL)/% |
|---|---|---|---|
| As-received | 425 | 320 | 11.2 |
| Un-coated, 80% loaded | 420 | 348 | 3.5 |
| MAO coated, 80% loaded | 426 | 365 | 10.5 |
| Uncoated, pre-exposed | 432 | 386 | 2.5 |

coated alloy specimen (Fig. 10). Furthermore, the fracture morphology of the specimen exhibits clear ductile cracking morphology without any intergranular separation, suggesting the absence of susceptibility to SCC in both the cases (Fig. 11). Based on the ductile cracking morphology along with poor elongation of the pre-exposed samples of the uncoated alloy, it can be said that the reduction in elongation after constant load SCC tests could be due to the localized corrosion leading to mechanical overload failure and not due to SCC.

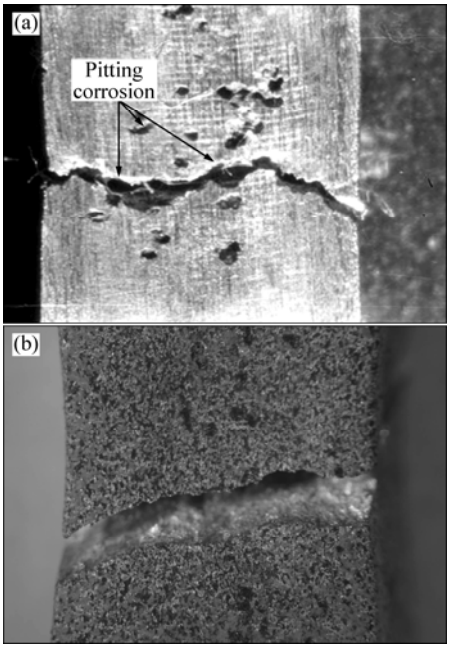


**Fig. 10** Stereo microphotographs showing severe pitting on uncoated specimen (a) and distribution of pores on MAO coated specimen observed after SCC tests (b)

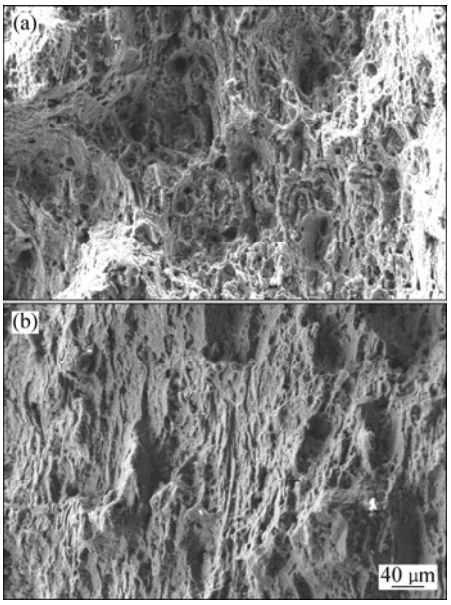


**Fig. 11** Fracture morphology of un-coated (a) and MAO coated AA7075 alloy (b) observed after constant load SCC exposure followed by tensile test

## 4 Discussion

The results of the present study show that the alumina coating generated on AA7075 aluminium alloy using dilute alkali−silicate electrolyte exhibits a

two-layer structure with an outer porous and inner compact layers, which is consistent with the reported results of similar PEO coated aluminium and magnesium alloys [17,19]. The variation in resistance values $R_P$ and $R_B$ of the coated sample clearly reflects the differences in the electrochemical behaviour of the porous and compact oxide layers with respect to the corrosion protection of the base metal. The drastic reduction in $R_P$ value after 0.5 h indicates that the electrolyte quickly diffuses through the outer layer in view of the large number of pores and reaches the inner compact layer. Although a similar decreasing trend is observed in $R_B$ values, they are very high compared with $R_P$ values measured for the porous layer at all immersion time. This demonstrates that the inner compact layer only offers the corrosion protection for the base alloy and thereby prevents the localized corrosion. XUE et al [12] through elemental analysis across the cross section of the coating performed after corrosion tests detected the presence of chloride ions only in the porous layer and not in the compact inner layer. Hence the corrosion resistance of the MAO coating is mainly derived from the inner compact layer. The evolution of impedance spectra with time, in general shows good correlation between the morphology of the oxide coating and the corrosion performance over a period of time.

Despite the good SCC resistance of this alloy in the over aged condition [23−25], the significant reduction in elongation values for the uncoated tensile sample after constant load SCC test can be attributed to the localized pitting corrosion resulting in mechanical overload cracking rather than true SCC. Severe localized corrosion is clearly evident on the macro photograph of the tensile sample observed after SCC test. In addition, the poor elongation of the pre-exposed samples further supports that the failure is not due to SCC. However, the role of hydrogen cannot be ruled out in spite of the ductile cracking of the alloy as hydrogen evolution is possible in the presence of Fe- and Cu-containing cathodic phases in aluminium. This needs to be studied in detail. It can also be noted that, the coated specimen exhibits noticeable elongation as a result of the absence of such localized corrosion and thus maintains the elongation value of the uncoated as-received sample. The results are in agreement with the published results on magnesium alloy coated with alumina towards improving the ductility of the alloy in the corrosive environment [26]. It was also reported that, such coating could not completely prevent the stress corrosion cracking on those alloys. This is mainly due to the more reactive nature of magnesium compared with aluminium alloy used in the present study in the over aged condition. The results obtained in the present study clearly show the improvement in localized corrosion resistance of AA7075 aluminium alloy, thereby the improved ductility especially the good barrier protection due to the inner oxide layer.

The XRD results revealed only $\gamma$-$Al_2O_3$, and the reported results on other aluminium alloys showed the presence of both $\alpha$ and $\gamma$-$Al_2O_3$ phases together [9,10]. This could be due to the higher Mg and Zn content present in this alloy. As they were reported to increase the transition temperature of $\gamma$- to $\alpha$-$Al_2O_3$ phase during the cooling process of the coating, resulting in predominant $\gamma$-$Al_2O_3$ phase. Another possible reason for the absence of $\alpha$-$Al_2O_3$ phase in the present work could be due to the lower silicon content used in the electrolyte. It was reported that silicon accelerates the growth rate of the coating, resulting in higher thickness of the coating [16]. The higher the thickness of the coating, the lower the cooling rate and hence the higher the $\alpha$-$Al_2O_3$ content. Although EDS analysis revealed the presence of $SiO_2$ in the outer surface of the coating, the absence of such phase in the XRD analysis could be due to the fewer amounts of the respective oxides to be identified by XRD.

## 5 Conclusions

1) Ceramic alumina coating by micro arc oxidation method offered good barrier effect in chloride environment on improving the localized corrosion resistance of AA7075 aluminium alloy under long-term immersion conditions.

2) The impedance results satisfactorily explained the behaviour of the coating and have been modelled with appropriate equivalent circuits.

3) The constant load SCC test results clearly revealed the role of localized corrosion on the reduction in elongation of the alloy and its improvement by the coating.

## Acknowledgments

The authors A. Venugopal, S. Manwatlear and K. Sreekumar are grateful to Dr. P. P. Sinha, deputy director, MME, and VSSC for the interest and encouragement shown in this work.

## References

[1] ANDRETTA F, TERRYN H, de WIT J H W. Effect of solution treatment on galvanic coupling between intermetallics and matrix in AA7075-T6 [J]. Corros Sci, 2003, 45: 1733−1746.

[2] PAO P S, Gill S J, FENG L R. On fatigue crack initiation from corrosion pits in 7075-T7351 aluminium alloy [J]. Scripta Materialia, 2000, 43(5): 391−396.

[3] BIRBILIS N, CVANAUHG M K, BUCHHEIT R G. Electrochemical behaviour and localized corrosion associated with $Al_7Cu_2Fe$ particles in aluminium alloy 7075-T651 [J]. Corros Sci, 2006, 48: 4202−4215.

[4] WLOKA J, BURKLIN G, VIRTANEN S. Influence of second phase

particles on initial electrochemical properties of AA7010-T76 [J]. Electrochemica Acta, 2007, 53: 2055−2059.
[5] WEI R P, LIAO C M, METALL G M. A transmission electron microscopy study of constituent particle induced corrosion in 7075-T6 and 2024-T3 aluminum alloys [J]. Metall Trans A, 1998, 29: 1153−1160.
[6] GAO M, FENG C R, WEI R P. An analytical electron microscopy study of constituent particles in commercial 7075-T6 and 2024-T3 alloys [J]. Metall Trans A, 1998, 29: 1145−1152.
[7] CHEN G S, WAN K C, GAO M, WEI R P, FLOURNOY T H. Transition from pitting to fatigue crack growth modelling of corrosion fatigue crack nucleation in a 2024-T3 aluminium alloy [J]. Mat Sci & Eng A, 1996, 219: 126−132.
[8] SANKARAN K K, JOHNSOR B, PEREZ R, JATA K V. Proceedings of the 1997 Tri-Service Conf. On Corrosion. NSWC, Bethesda, MD, 1998.
[9] OH Young-Jun, MUN Jung-II, KIM Jung-Hwan. Effects of alloying elements on microstructure and protective properties of $Al_2O_3$ coatings formed on aluminium alloy substrates by plasma electrolysis [J]. Surf & Coat Technol, 2009, 204: 141−148.
[10] TILLOUS K, TOLL-DOUCHANOY T, BAUER-GROSSE E, HERICHER L, GEANDIER G. Microstructure and phase composition of micro arc oxidation surface layers formed on aluminium and its alloys 2214-T6 and 7050-T74 [J]. Surf. & Coat. Technol, 2009, 203: 2969−2973.
[11] PRASAD RAO K, JANAKI RAM G D, STUCKER B E. Improvement in corrosion resistance of friction stir welded aluminium alloys with micro arc oxidation coatings [J]. Scripta Materialia, 2008, 58: 998−1001.
[12] XUE Wen-bin, WANG Chao, TIAN Hua, LAI Yong-chun. Corrosion behaviours and galvanic studies of micro arc oxidation films on Al-Zn-Mg-Cu alloys [J]. Surf & Coat Technol, 2007, 201: 8695−8701.
[13] ASQUITH D T, YEROKHIN A L, YATES J R, MATTHEWS A. The effect of combined shot-peening and PEO treatment on the corrosion performance of 2024 aluminium alloy [J]. ThinSolid Films, 2007, 516: 417−421.
[14] RAJASEKARAN B, GANESH SUNDARA RAMAN S, RAMA KRISHNA L, JOSHI S V, SUNDARARAJAN G. Influence of micro arc oxidation and hard anodizing on plain fatigue and fretting fatigue behaviour of Al−Mg−Si alloy [J]. Surf & Coat Technol, 2008, 202: 1462−1469.
[15] LIANG J, BALA SRINIVASAN P, BLAWERT C, DIETZEL W. Comparison of electrochemical behaviour of MgO and $ZrO_2$ coatings on AM50 magnesium alloy formed by plasma electrolytic oxidation [J]. Corros Sci, 2009, 51: 2483−2492.
[16] LI H X, RUDNEV V S, ZHENG X H, YAROVAYA T P, SONG R G. Characterization of $Al_2O_3$ ceramic coatings on 6063 aluminium alloy prepared in borate electrolytes by micro arc oxidation [J]. Journal of Alloys and Compounds, 2008, 462: 99−102.
[17] GHASEMI A, RAJA V S, BLAWERT C, DIETZEL W. Study of the structure and corrosion behaviour of PEO coatings on AM50 magnesium alloy by electrochemical impedance spectroscopy [J]. Surf & Coat Technol, 2008, 202: 3513−3518.
[18] BALA SRINIVASAN P, BLAWERT C, DIETZEL W. Effect of plasma electrolytic oxidation coating on the stress corrosion cracking behaviour of wrought AZ61 magnesium alloy [J]. Corros Sci, 2008, 50: 2415−2418.
[19] BALA SRINIVASAN P, BLAWERT C, DIETZEL W. Effect of plasma electrolytic oxidation treatment on the corrosion and stress corrosion cracking behaviour of AM50 magnesium alloy [J]. Mat Sci & Eng A, 2008, 494: 401−406.
[20] YEROKHIN A L, NIE X, LEYLAND A, MATHEWS A, DOWEY S. Plasma electrolysis for surface engineering [J]. Surf & Coatings Technol, 1999, 122: 73−93.
[21] CURRAN J A. CLYNE T W. Thermo-physical properties of plasma electrolytic oxide coatings on aluminium [J]. Surf & Coat Technol, 2005, 199: 177−183.
[22] WANG H, AKID R. A room temperature cured sol-gel anticorrosion pre-treatment for aluminium 2024-T3 alloy [J]. Corros Sci, 2007, 49: 4491−4503.
[23] SPEIDEL M O. Stress corrosion cracking of aluminium alloys [J]. Metall Trans A, 1975, 6: 631−652.
[24] DORWARD R C, HASSE K R. Flaw growth in high strength Al−Zn−Mg−Cu alloys exposed to stress corrosion environments [J]. Corrosion, 1978, 34: 386−395.
[25] PARKER J K, ARDELL A J. Effect of retrogression and re-aging treatments on the microstructure of aluminium 7075-T651 [J]. Metall Trans A, 1984, 15: 1531−1542.
[26] BALA SRINIVASAN P, SETTLER R, BLAWERT C, DIETZEL W. A study of the effect of plasma electrolytic oxidation on the stress corrosion cracking behaviour of a wrought AZ61 magnesium alloy and its friction stir weld [J]. Materials Characterization, 2009, 60: 389−396.

# 微弧氧化处理对 AA7075 铝合金在 3.5% NaCl 溶液中局部腐蚀行为的影响

A. VENUGOPAL[1], Rajiv PANDA[1], Sushant MANWATKAR[1], K. SREEKUMAR[1],
L. RAMA KRISHNA[2], G. SUNDARARAJAN[2]

1. Material Characterization Division, Materials and Metallurgy Group,
Vikram Sarabhai Space Centre, Thiruvananthapuram- 695022, India;
2. International Advanced Research Centre for Powder Metallurgy and New Materials, Hyderabad- 500005, India

**摘　要**：采用微弧氧化法在AA7075铝合金上生成氧化铝膜层，并对氧化铝膜层在3.5% NaCl溶液中的腐蚀和应力腐蚀开裂行为进行测试。采用电化学阻抗谱来研究膜层随浸泡时间的变化，构建合适的等效电路图。对常载荷应力腐蚀开裂测试后的试样进行金相观察。结果表明，微弧氧化膜可以有效避免富Cu、Fe金属间化合物相引发的严重局部腐蚀而导致的合金过早失效。

**关键词**：铝合金；微弧氧化；阻抗谱；应力腐蚀

**(Edited by YANG Hua)**